Title

Colloidal structure and proton conductivity of the gel within the electrosensory organs of cartilaginous fishes.

Journal

iScience, 24(9)

ISSN

2589-0042

Authors

Phillips, Molly

Wheeler, Alauna C

Robinson, Matthew J

et al.

Publication Date

2021-09-01

DOI

10.1016/j.isci.2021.102947

iScience

CellPress
OPEN ACCESS

Article

Colloidal structure and proton conductivity of the gel within the electrosensory organs of cartilaginous fishes

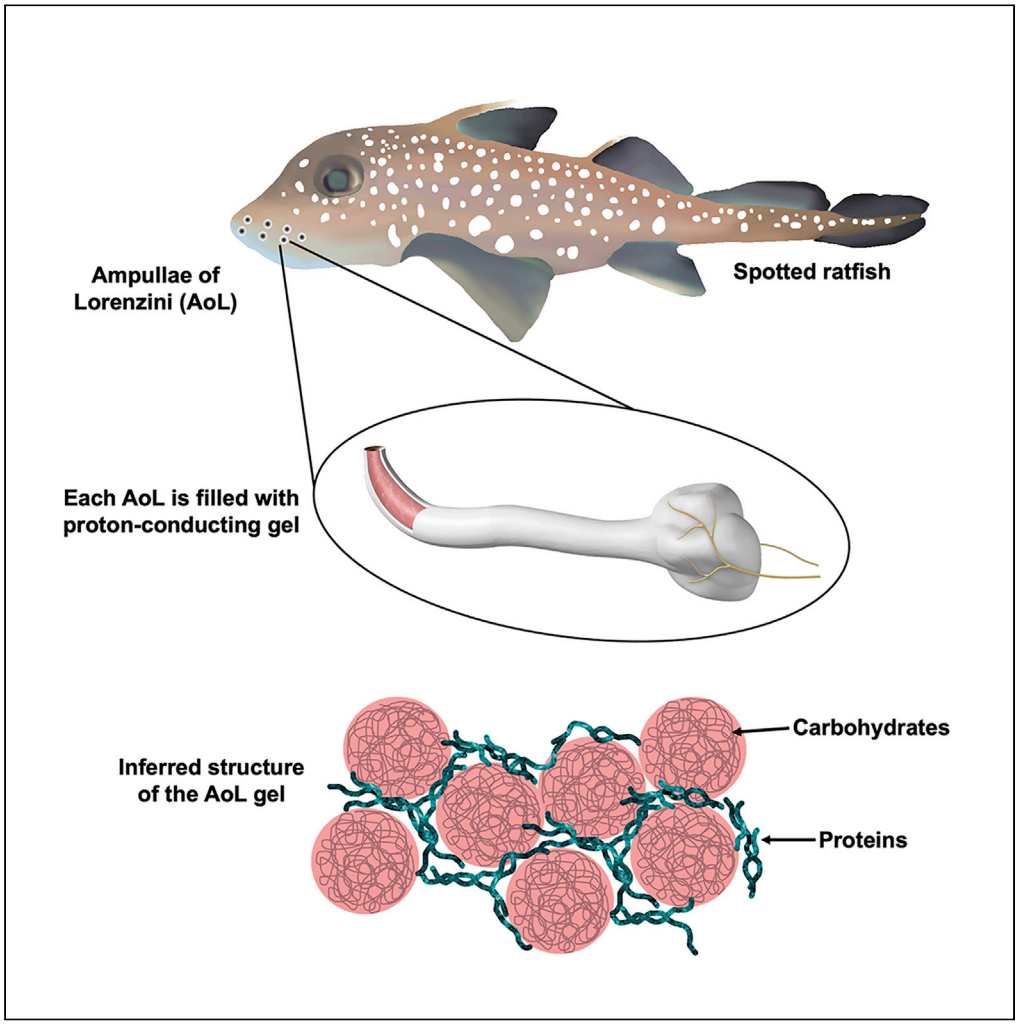

Molly Phillips, Alauna C. Wheeler, Matthew J. Robinson, ..., Marco Rolandi, Linda S. Hirst, Chris T. Amemiya

lhirst@ucmerced.edu (L.S.H.)
camemiya@ucmerced.edu (C.T.A.)

Highlights

SEM and AFM of the gel from ratfish electrosensory organs reveal a globular structure

Analysis of the gel by SAXS suggests a distinct, colloidal substructure

High proton conductance was observed in the gel, comparable with that of sharks and skates

Proteolysis breaks up large-scale aggregates but has little effect on proton conductance

Phillips et al., iScience 24, 102947
September 24, 2021 © 2021
https://doi.org/10.1016/j.isci.2021.102947

iScience

CellPress
OPEN ACCESS

Article

Colloidal structure and proton conductivity of the gel within the electrosensory organs of cartilaginous fishes

Molly Phillips,[1,2] Alauna C. Wheeler,[3] Matthew J. Robinson,[4] Valerie Leppert,[4] Manping Jia,[5] Marco Rolandi,[5] Linda S. Hirst,[3,6,*] and Chris T. Amemiya[1,2,6,7,*]

SUMMARY

Cartilaginous fishes possess gel-filled tubular sensory organs called Ampullae of Lorenzini (AoL) that are used to detect electric fields. Although recent studies have identified various components of AoL gel, it has remained unclear how the molecules are structurally arranged and how their structure influences the function of the organs. Here we describe the structure of AoL gel by microscopy and small-angle X-ray scattering and infer that the material is colloidal in nature. To assess the relative function of the gel's protein constituents, we compared the microscopic structure, X-ray scattering, and proton conductivity properties of the gel before and after enzymatic digestion with a protease. We discovered that while proteins were largely responsible for conferring the viscous nature of the gel, their removal did not diminish proton conductivity. The findings lay the groundwork for more detailed studies into the specific interactions of molecules inside AoL gel at the nanoscale.

INTRODUCTION

Electroreception, the ability of some animals to detect electric fields, is widespread among vertebrates. Some of the most well-studied electroreceptive animals are rays, skates, sharks, and chimaeras – cartilaginous fishes of the class Chondrichthyes. These fishes use specialized electrosensory organs for the detection of low-frequency electric fields from biological sources such as prey or mates, and even for navigating using earth's geomagnetic field (Kalmijn, 1974; Newton et al., 2019; Tricas et al., 1995). These electrosensory organs, called Ampullae of Lorenzini (AoL), are observable externally as small pores that are open to the surrounding environment (Figure 1A). In sharks and chimaeras, pores are most concentrated on the snout and around the mouth, whereas in skates and rays, they are more widespread across the ventral and dorsal surfaces of the animals (Kempster et al., 2012; Raschi, 1986). AoL pores lead into tubular collagen-wrapped canals of varying lengths and diameters (depending on species and location on the body) that are lined on the inside by two layers of epithelial cells. At the distal end of each canal is a bulbous alveolus containing electrosensory hair cells that synapse with neurons connected to the medulla of the brain (Figure 1B). Importantly, the organs are filled with a viscoelastic gel that can be extracted by applying pressure to the skin adjacent to AoL pores and subjected to biophysical examination (Figure S1). While the sensory capabilities of the AoL have been studied in detail over the past several decades, the process by which signals move from the environment through the organs, and how the gel is involved, remains a subject of debate (Newton et al., 2019).

Research in the 1960s showed that AoL gel is approximately 95% water containing Na^+, K^+, Cl^-, and urea (Murray and Potts, 1961). By measuring the relative abundances of hexosamines, sulfates, and other chemical groups, researchers identified that the gel contains various "mucopolysaccharides," but the specific identities of these components have remained unknown until recent years (Doyle, 1967). AoL gel extracted from three fish species demonstrated extremely high proton conductivity, higher than that of any other reported biological material (Josberger et al., 2016). It has been proposed that keratan sulfate, a glycosaminoglycan, is a component of AoL gel and responsible for conferring the substance's proton conductive properties (Josberger et al., 2016; Zhang et al., 2018). Various studies have attempted to uncover the molecular makeup of AoL gel, most with a focus on polysaccharides and proteins (How and Jones, 1969; How et al., 1970; Zhang et al., 2018). Cellular contamination during AoL gel extraction, however, makes the

[1]Department of Biology, University of Washington, Seattle, WA 98195, USA

[2]Department of Molecular and Cell Biology, University of California, Merced, Merced, CA 95343, USA

[3]Department of Physics, University of California, Merced, Merced, CA 95343, USA

[4]Department of Materials Science and Engineering, University of California, Merced, Merced, CA 95343, USA

[5]Department of Electrical and Computer Engineering, Baskin School of Engineering, University of California, Santa Cruz, Santa Cruz, CA 95064, USA

[6]Quantitative and Systems Biology Program, University of California, Merced, Merced, CA 95343, USA

[7]Lead contact

*Correspondence: lhirst@ucmerced.edu (L.S.H.), camemiya@ucmerced.edu (C.T.A.)

https://doi.org/10.1016/j.isci.2021.102947

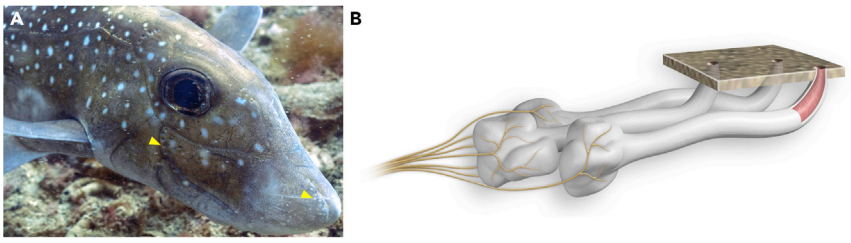

Figure 1. Anatomy of Ampullae of Lorenzini (AoL)

(A) An image showing a type of chimaera called a spotted ratfish (*Hydrolagus colliei*). Yellow arrowheads delineate the locations of some AoL pores. Image taken by Mick Otten.

(B) A diagram showing three AoL below the skin surface. Pores lead into canals filled with a gel (as made visible by the cutaway). Neurons (yellow) synapse with specialized electrosensory cells in the alveoli and project onto the hindbrain.

interpretation of proteomic data sets challenging. We recently reported evidence suggesting that chitin is another polysaccharide component of the gel, but it remains unknown if the chitin molecules are modified in some way or complexed with other components in order to promote solubility in the aqueous gel (Phillips et al., 2020).

Major gel-forming components have been shown to exist as fibrous or rod-like particles, flexible coils, spherical particles, or linear molecules held together by crystalline junctions (Djabourov, 1988). However, it is still unclear how the molecular components of AoL gel are arranged and how they contribute to the gelatinous nature of the material. Furthermore, it is unknown how the gel's viscoelastic structure factors into the proton conductivity of the substance. Using data from proteomics and polysaccharide analyses, Zhang *et al.* proposed a hypothetical model of AoL gel structure consisting of actin filaments holding together a scaffold of mucins bound to keratan sulfate molecules (Zhang et al., 2018). Zhang *et al.* based their model on inferred interactions of gel components that they identified using chemical extraction methods and proteomics; the model was not based on biophysical structural data. Here, we describe an entirely different approach to studying the structure of AoL gel samples from spotted ratfish (*Hydrolagus colliei*) (Figure 1A) by small-angle X-ray scattering (SAXS), scanning electron microscopy (SEM), and atomic force microscopy (AFM). To understand the influence of the gel's protein component specifically, we digested gel with the proteolytic enzyme, proteinase K, and compared the gross morphology and scattering properties of gel before and after protein removal. Furthermore, we studied the influence of proteins on the proton conductivity of the material using electrochemical impedance spectroscopy. Our results, *in toto*, suggest a different model for the gel structure than had previously been suggested.

RESULTS

Description of AoL gel using fluorescence microscopy

Low-magnification fluorescence microscopy was used to study the structure of formalin-fixed tissues from spotted ratfish (*H. colliei*) that were stained with fluorescent probes consisting of a chitin binding domain (CBD) (Phillips et al., 2020; Tang et al., 2015) (Figures 2A and 2B). CBD detects chitin within AoL gel material in a highly specific manner (Phillips et al., 2020) and served as a marker of the fine outlines of the gel. The gel of sectioned AoL was organized into small packets that looked to be extruded from individual cells (Figure 2B). Importantly, it is unclear how much of the observed structure resulted from fixation. To overcome this, we also stained native AoL gel extracted from *H. colliei* with CBD and imaged with fluorescence microscopy to reveal a sheet-like macroscopic structure (Figures 2C and 2D). The shape of the gel's structure was reminiscent of the wrinkled appearance of other biopolymer gels (Hirst et al., 2005). All experiments described hereafter used native, unfixed gel material.

Analysis of AoL gel by AFM and SEM

To study the structure of AoL gel at higher magnifications, we used AFM and SEM. When imaging *H. colliei* AoL gel with AFM, abundant spherical globules were observed at various locations across the mica surface (Figures 3A and 3B). These globular structures were often piled on top of one another (inset of Figure 3A) and in some cases appeared to combine to form large aggregates. An average globule had a diameter of approximately 100 nm. The globules appeared to be closely associated and buried in a mat that covered

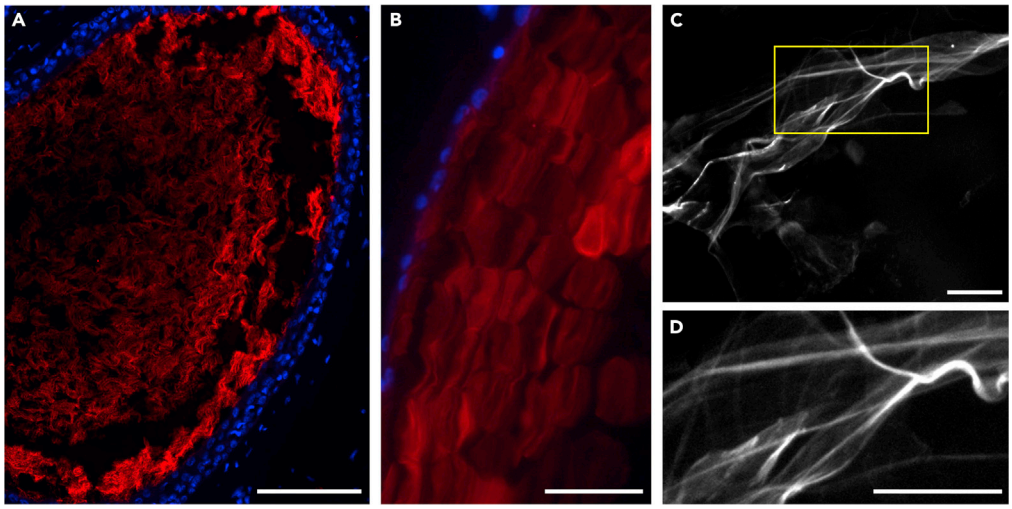

Figure 2. Visualization of spotted ratfish (*Hydrolagus colliei*) AoL gel via fluorescence microscopy

(A and B) Formalin-fixed paraffin tissue sections from two different *H. colliei* specimens imaged with fluorescence microscopy. Tissues were stained with chitin-binding CBD probes (red) as well as nuclear stain (DAPI, blue). Images show cross sections through AoL with increasing magnification from (A) to (B). DAPI-labeled nuclei line the edges of the canals and CBD-labeled gel fills the acellular canal lumens.

(C and D) Aqueous unfixed AoL gel from *H. colliei* labeled with CBD (white) and imaged with fluorescence microscopy. Area delineated by the yellow rectangle in (C) is shown at higher magnification in (D). Scale bars – A: 100 μm; B-D: 50 μm.

the mica. When smaller AFM scan areas were used, rope-like objects could also be seen weaving in between the globules (Figure 3B).

When freshly isolated gel was deposited on an aluminum stub, no consistent features were observed with SEM. Therefore, knowing that AoL gel is mostly water (Murray and Potts, 1961), ultracentrifugation was used to concentrate gel components and separate them from water. Pelleted AoL gel material was smeared across a piece of mica and then imaged with SEM at various magnifications (Figures 3C and 3D). At lower magnification, dense aggregated material was observed in dispersed mounds (Figure 3C). When higher magnification was used, globules of similar shape and size to those observed with AFM were resolved (Figure 3D). The shape of the objects observed with both AFM and SEM led us to suspect that AoL gel is colloidal in nature and composed of spherical particles. However, desiccation undoubtedly had some impact on the AoL gel structure, as drying effects have been shown to reduce the natural porosity of gel materials (Buchtova and Budtova, 2016; Ganesan et al., 2016).

To overcome the inevitable effects of desiccation on the AoL gel structure, we used SEM to image gel samples that had been exposed to supercritical CO_2. The supercritical dried sample exhibited a fine porous network similar in form to published images of so-called aerogels (Figure S2A) (Ganesan et al., 2018; Quignard et al., 2008). Aerogels are produced when hydrogel is dried in a manner that allows for the maintenance of the original form, such as by supercritical drying (Sahin et al., 2017). Given this, the SEM images of supercritical dried gel are likely more representative of aqueous gel structure than those SEM images of dried and vacuum dessicated gel. Close examination of the supercritical dried gel structure revealed various structural arrangements, some densely packed and solid (Figure S2B), but most porous and loose (Figure S2C). In all cases, the gel structure appeared to consist of globular elements that were on average 100–200 nm in diameter. These findings are consistent with the proposition that AoL gel is colloidal and composed of aggregating spherical objects.

Comparison of microscopic structure and X-ray scattering properties of AoL gel before and after digestion with proteinase K

Next, we wanted to investigate which macromolecular gel components comprised the spherical globules observed by microscopy. Knowing that AoL gel is composed primarily of polysaccharides and proteins, we digested aliquots of gel from *H. colliei* with proteinase K and studied the properties of the material that

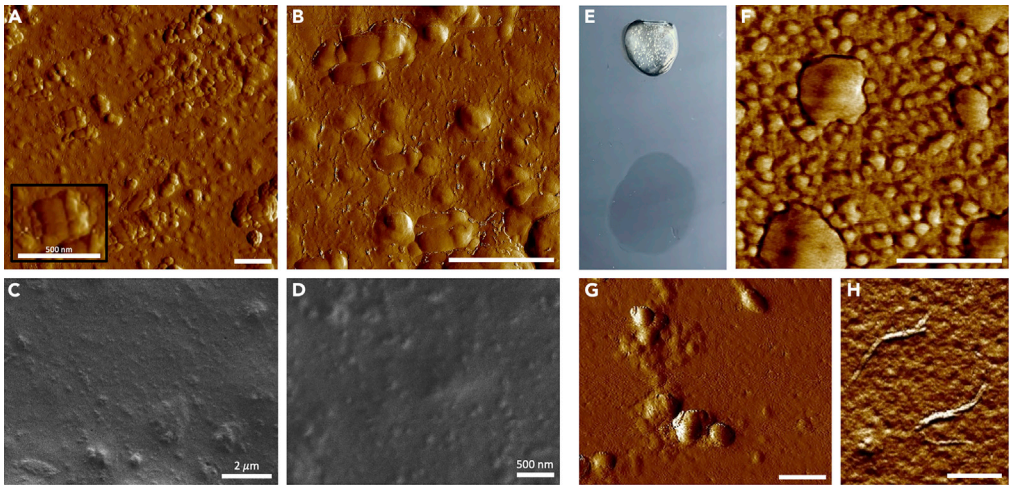

Figure 3. Microscopic analysis of AoL gel before and after digestion with proteinase K

(A and B) AoL gel from *H. colliei* was diluted by 1/20 with water, dropped on a freshly cleaved mica sheet, air-dried, and imaged with AFM. Globular structures were observed widespread across the surface (A). The inset in (A) magnifies one region of the image where the globules exhibit organized packing. Closer examination of the gel using AFM revealed rope-like objects winding in between the globules (B).

(C and D) Pellet resulting from ultracentrifugation of AoL gel was dragged across a freshly cleaved piece of mica then imaged with SEM. Images show the same sample (in slightly different fields) at lower (C) and higher (D) magnification. The majority of the surface was covered in a mat of material which, at higher magnification, appeared to be composed of globules comparable in size with those observed with AFM.

(E) Image showing a fresh aliquot of *H. colliei* AoL gel (top) above a drop of proteinase-K-treated *H. colliei* gel (bottom) demonstrating the qualitative reduction in material viscosity following protein digestion.

(F) AFM image showing a sample of *H. colliei* gel that had been digested with proteinase K, diluted by 1/20 with water, and dropped onto a freshly cleaved mica sheet to ambiently dry. We observed globules spread across the mica surface similar in appearance to those globules observed in the nondigested gel samples. Linear rope-like structures were not apparent in the digested sample

(G) AFM image showing a sample of *H. colliei* gel that had been digested with proteinase K, dialyzed with 12- to 14-KDa tubing, then dropped and ambiently dried on freshly cleaved mica. Despite the definite reduction in protein material as evidenced by sodium dodecyl sulphate–polyacrylamide gel electrophoresis (SDS-PAGE) (Figure S3), aggregating globules were still clearly observed.

(H) Amplitude AFM image showing whisker-like crystalline structures resulting from sonication of the same sample of proteinase-K-digested AoL gel that is shown in (G). Scale bars – A, B, D, F-H: 500 nm; C: 2 μm.

remained after digestion. Remarkably, after one hour of proteinase K exposure, the AoL gel transitioned into a fluid state. This phenomenon was demonstrable when samples were dropped onto a glass slide before and after digestion (Figure 3E). To assess the efficacy of enzymatic digestion, we analyzed samples of native and digested AoL gel using SDS-PAGE and observed a marked reduction in detectable protein before and after treatment with proteinase K (Figure S3). Using tubing with ~14-KDa molecular weight cut-off, we dialyzed an aliquot of digested AoL gel, revealing an even greater reduction of proteins (Figure S3). When digested gel was imaged with AFM, we observed globules similar to those that were seen comprising native AoL gel (Figures 3F and 3G). These globules were visible both in undialyzed (Figure 3F) and dialyzed (Figure 3G) samples. Additionally, when a sample of proteinase-K-digested gel was sonicated prior to AFM imaging, the material took on an entirely new form (Figure 3H). Interestingly, the structures resulting from sonication resembled published images of chitin crystals generated by chemically extracting polysaccharides from AoL gel (Figures 3H and S4), indicating that chitin likely composes at least some portion of the globules (Phillips et al., 2020).

Microscopic evidence suggested that samples of native and proteinase-K-digested AoL gel were composed of aggregating spherical particles. However, while globules appeared to be in tight mat-like association in native gel samples (Figures 3A and 3B), they looked more dissociated in digested gel (Figures 3F and 3G). Therefore, we next asked if there were differences in the internal structure of the globules in aqueous solutions of native and digested AoL gel. To address this question, we performed SAXS on AoL gel before and after proteinase K digestion. SAXS analyses are ideal for studying poorly ordered dilute

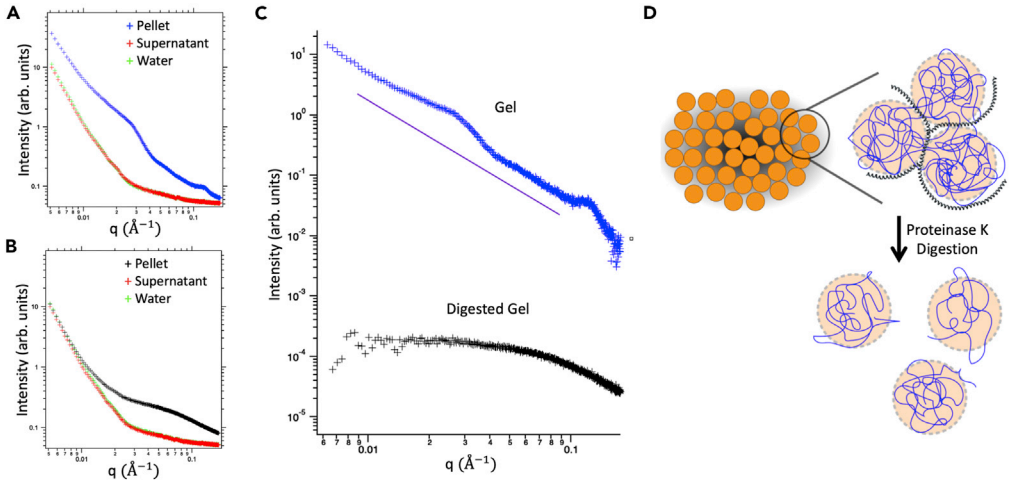

Figure 4. Comparison of native *H. colliei* AoL gel and proteinase-K-digested AoL gel by SAXS

(A and B) Scattering intensity is plotted as a function of the scattering vector, *q*. SAXS data using material resulting from ultracentrifugation of untreated AoL gel (A) and proteinase-K-digested AoL gel (B).

(C) Comparison of SAXS data from native gel pellet and the digested gel's light cloudy material. Both plots are shown with water background subtracted. The purple line indicates a slope of −2 as a guide to the eye.

(D) Hypothetical model of AoL gel structure based on microscopy and SAXS. Globules observed with SEM and AFM are depicted in orange. Polysaccharide polymers (blue) are packed into rough spherical shapes that are held in close association by proteins (represented by black coils) when gel is in its native state (top). Digestion with proteinase K breaks up the majority of these proteins (bottom) which leads to fluidization of the gel.

aqueous materials such as AoL gel (Stribeck, 2007). Because the gel is composed primarily of water, we first ultracentrifuged our samples to concentrate the major macromolecular components. Ultracentrifugation of native gel yielded a thick white pellet, while digested gel formed a yellowish cloud at the bottom of the centrifuge tube. Both tubes contained a sizable proportion of clear supernatant. The supernatant and the concentrated material from both samples were placed in a thin-walled X-ray capillary tube before exposure to the X-ray beam. Figures 4A and 4B show SAXS scattering patterns from native gel and proteinase-K-digested gel, respectively. The supernatant from both gel samples exhibited scattering patterns extremely similar to water, whereas the concentrated materials displayed some notable differences (Figures 4A and 4B). Differences were especially apparent after background scattering from water was subtracted from both samples. The resulting curves reflect scattering primarily from polymers and proteins existing in the gel materials (Figure 4C).

The scattering curve resulting from undigested AoL gel has a slope close to −2 on a log-log plot (Figure 4C, blue plot). One possible interpretation based on the magnitude of this slope is that the AoL gel components are organized similarly to an ideal polymer chain over length scales from ~6–90 nm. An ideal (Gaussian) polymer chain is freely jointed and self-avoiding, with characteristic scattering described by the Debye function, $S(q) \propto 1/q^{v}$ where *v* is exactly equal to 2 (Pethrick, 2004). For a self-avoiding chain, the value of *v* is slightly higher as the chain effectively swells. The purple line in Figure 4C shows a slope of −2 as a guide to the eye. The curve has a clear broad peak at $q = 0.028$ Å^{-1}, which corresponds to a real space length scale, *d* of 22 nm (where $q = \frac{2\pi}{d}$). This peak may represent a length scale related to the average separation of the globules in the gel. A second peak can also be observed at approximately 0.1 Å^{-1}, corresponding to a real space length scale of $d = 5$ nm, and we hypothesize that this peak is explained by the presence of some cellular debris within the gel, namely cell membranes, which are on average approximately 5 nm in thickness (Phillips, 2018).

In contrast, the concentrated proteinase-K-digested sample produced a scattering curve with no obvious peaks that levels off at a low *q*, indicating a lack of large-scale aggregated structures in the cloudy material resulting from ultracentrifugation. The curve is reflective of the material's structure after digestion (Figure 4C, black plot) and suggests that the polymers remaining in the gel after digestion lack an organized arrangement and are likely dilute. A model summarizing our analysis of these findings is shown in Figure 3D and is consistent with our microscopy results.

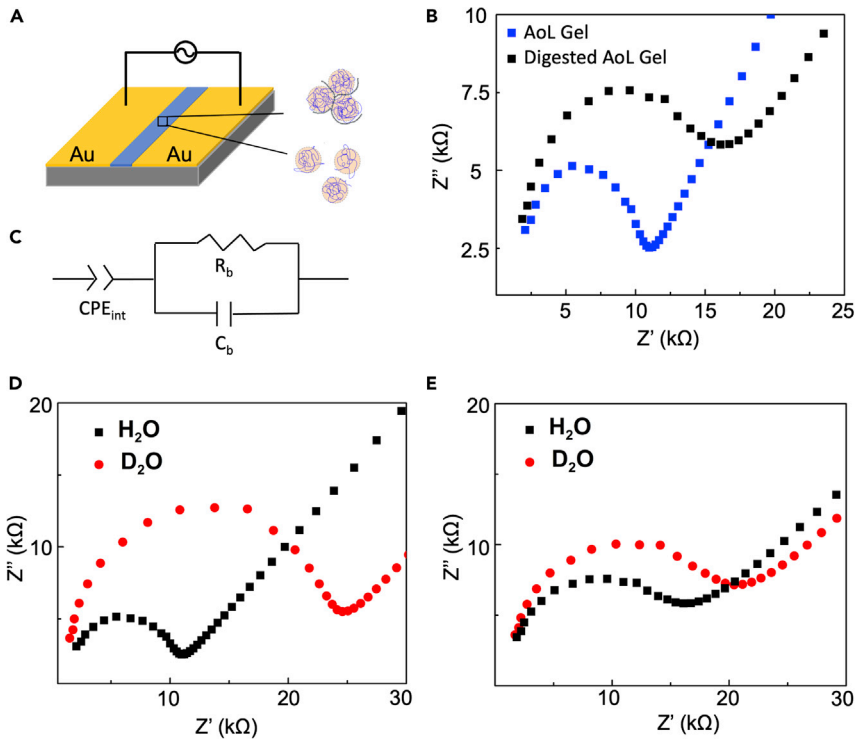

Figure 5. Proton conductivity of *H. colliei* AoL gel before and after proteinase K digestion

(A) Two-terminal device used for EIS measurement.

(B) Nyquist plots of native AoL gel (blue) and digested AoL gel (black) at 90% relative humidity.

(C) Equivalent circuit model. A constant phase element (CPE) was used to describe the nonideal interface capacitance; Rb and Cb represent the resistance and capacitance of the sample, respectively.

(D and E) Nyquist plots of native *H. colliei* AoL gel (D) and proteinase-K-digested *H. colliei* AoL gel (E) in the presence of H_2O vapor (black) and D_2O vapor (red).

Proton conductivity of AoL gel before and after digestion with proteinase K

Finally, in order to develop an understanding of the functional differences between AoL gel before and after proteolytic digestion, we compared the proton conductivity of native AoL gel from *H. colliei* and proteinase-K-treated gel with alternating current (a.c.) electrochemical impedance spectroscopy (EIS) (Figure 5A). Both gel samples were dialyzed against H_2O before measurements to remove other ions that could contribute to the conductivity. The Nyquist plots of both native and digested AoL gel show semicircles in the high-frequency region and an inclined spur in the low-frequency region (Figure 5B). These features are fingerprints of materials with predominant ionic conductivity (Bureekaew et al., 2009). We calculated the conductivity using a simple equivalent circuit (Figure 5C) (Guo et al., 2020; Jalili and Tricoli, 2014; Soboleva et al., 2008). For native AoL gel, we calculated the effective conductivity to be 5 ± 3.5 mS cm^{-1}, which is consistent with the value of the conductivity (2 ± 1 mS cm^{-1}) of AoL gel from other cartilaginous fish species measured previously (Josberger et al., 2016) using transmission line measurement devices. Given the variability associated with samples extracted from biological specimens, the agreement of the values within the uncertainty range is remarkable. For the digested gel, we calculated the effective conductivity to be 22 ± 8.5 mS cm^{-1}. The sizable error observed with both measurements comes from the uncertainty associated in evaluating the thickness of gel material in the devices (Figure S5A). Regardless, it appears that the conductivity of the proteinase-K-digested material is higher than that of native AoL gel. To further confirm that the charge carriers in the gel are protons, we studied the kinetic isotope effect by loading the gel with H^+ and D^+ in water (H_2O) vapor and deuterium oxide (D_2O) vapor, respectively (Josberger et al., 2016). The resistance of both native and digested AoL gel in D_2O vapor was significantly higher than that in water as expected when protons dominate the conductance of the material because the mobility of D^+ is approximately half of the mobility of H^+ (Figures 5D and 5E). This result provides confirmation that AoL gel from *H. colliei* is a proton conductor at high relative humidity and corroborates our previously reported observations (Deng et al., 2013).

DISCUSSION

Evidence from microscopic examination suggested that AoL gel from *H. colliei* is colloidal in nature, with spherical globules comprising a substantial portion of the observable macromolecular structure. SAXS data using concentrated AoL gel revealed a scattering peak corresponding to a real-space length scale of 22 nm. Globules were still observable by AFM in proteolyzed gel samples, whereas the 22-nm peak was completely absent from the SAXS plot generated using the same material. Taken together, these findings suggest that the 22-nm peak represents a length scale related to the average separation of the spherical globules within AoL gel. In addition, for the undigested samples, the range of length scales over which we observed close to ideal chain behavior (6–90 nm) suggests that there is some degree of chain interdigitation between globules in the aggregated structure, producing a continuous polymer network. It is important to point out that ultracentrifugation may have impacted the size of the polymer globules in native AoL gel; therefore, the 22-nm peak would represent a lower correlation length limit. It should also be noted here that other polymer structures, such as fractal aggregates, may possibly give rise to scattering patterns similar to the one reported. Detailed model fitting procedures often used for SAXS data are precluded here owing to the unknown composition of the AoL gel, and thus, future experiments will be necessary to elucidate the internal structure of the globules in more detail.

When ambiently dried AoL gel was imaged with AFM, rope-like structures were observed weaving among the globules (Figures 3A and 3B). These structures were absent in proteinase-K-digested gel, which suggests that they consist of proteins involved in holding the polymer network together. Elimination of these tethering proteins by enzymatic digestion seemingly collapsed the polymer network, and although the globules remained, they became dispersed randomly in solution (diagrammed in Figure 4D).

It is still unclear what materials compose the globules entirely. The fact that the globules were still clearly resolvable after proteinase K digestion makes it unlikely that they are highly composed of proteins. Therefore, the material remaining after proteinase K digestion could be composed of polysaccharides, lipids, or a combination of macromolecules. However, the globules comprising AoL gel resemble published images of chitosan nanoparticles (Haas et al., 2005); moreover, crystals reminiscent of chitin nanowhiskers were formed when the carbohydrate-extracted gel material was sonicated (Phillips et al., 2020; Zeng et al., 2012). These observations likely indicate that chitin makes up a substantial portion of the spherical globules, perhaps functioning as a scaffold that organizes proton-conductive keratan sulfate molecules.

By comparing the proton conductivity of native and proteinase-K-digested ratfish gel, we learned that proteins may not play a direct role in the conductivity of the material, despite their clear contribution to the gel's observed viscosity. In prior work (Josberger et al., 2016), we speculated that sulfated polysaccharides, namely keratan sulfate molecules, were responsible for conferring the observed proton conductivity of AoL gel. If we consider the gel as a mixture of highly conductive polysaccharides (Selberg et al., 2019) and less conductive proteins, removing the proteins should lead to a more conductive material as observed here. Nonetheless, the fact that the digested gel is more conductive than native gel confirms that proteins are not directly responsible for the observed proton conductivity. These data, along with the SAXS spectra, do not indicate which specific proteins play a role in the gel's structure and function. However, our results suggest that proteins do confer the gelatinous nature of the material and contribute to the maintenance of the structured polymer network but are not critical for proton conductivity. Interestingly, we noticed that approximately one out of four measurements on the digested gel sample contains a Nyquist plot that hints at the presence of two semicircles at high and mid frequencies as well as a clear polarization spike at low frequency (Figure S5B). Potential reasons for the presence of two semicircles include grain boundary between globules (Irvine et al., 1990; Maier, 2005) or a nonuniform current distribution (Harm et al., 2019). It is possible that the lack of an organized structure in the digested gel may affect the proton conduction and give rise to the two semicircles. This observation also suggests that the proteins may play an indirect role in the proton transport by organizing the polyglycans responsible for the proton conduction.

Finally, we note that our proposed model (Figure 4D) for the structure of the AoL gel is intrinsically different from that given by Zhang *et al.* (Zhang et al., 2018). This is, in part, due to differences in the data types used. The model of Zhang *et al.* was generated by inference using proteomics data from the AoL gel and presumptive scaffolding of keratan sulfate, conceptually similar to the bottle-brush model of aggrecan (Harder et al., 2010; Ng et al., 2003). In contrast, our model is based on AFM and SEM imaging along with corroborating SAXS spectral analysis and proposes a colloidal gel organization. We never observed anything

reminiscent of bottle-brush structures in AFM, and given the published sizes of such aggrecan bottle-brushes (≥200 nm) (Ng et al., 2003), we doubt that the globules are composed of smaller subunits of such structures. Regardless, it will be important to subject both models to further physicochemical and structural analyses in order to better deduce the underlying electrosensory mechanisms of the AoL of cartilaginous fishes.

Limitations of the study

To study the molecular makeup and structure of AoL gel, we needed to extract gel material from the tubular organs of deceased fish by applying physical pressure to the skin around the AoL pores. Therefore, all of the studies described here were limited by inevitable contamination of cellular and mucosal debris during the gel's extraction process. Because of this limitation, when studying the macromolecular components of AoL gel, we eliminated the gel's entire protein population as opposed to specific protein species. We also acknowledge that ultracentrifugation of gel samples used for SAXS may have introduced subtle changes to the scattering properties of the materials. Another limitation, as mentioned in the main text, was the need to desiccate AoL gel prior to imaging with AFM and SEM. It is unclear whether or not the observed features of desiccated gel reflect the native structure of aqueous gel. We used supercritical drying in an attempt to overcome this limitation. Finally, when we performed proton conductivity measurements, we filled two circular spacers with native gel and proteinase-K-digested gel. The native gel was extremely viscous, whereas the digested material was a liquid, and the two substances did not necessarily contain the same proportion of dissolved molecules.

STAR★METHODS

Detailed methods are provided in the online version of this paper and include the following:

- KEY RESOURCES TABLE
- RESOURCE AVAILABILITY
  - Lead contact
  - Materials availability
  - Data and code availability
- EXPERIMENTAL MODEL AND SUBJECT DETAILS
- METHOD DETAILS
  - Biological specimens
  - CBD staining and fluorescence microscopy
  - Gel digestion with proteinase K (for AFM imaging) and analysis by SDS-PAGE
  - Gel digestion with proteinase K (for SAXS)
  - Gel digestion with proteinase K (for sonication and AFM)
  - Ultracentrifugation of AoL gel
  - Synchrotron X-ray experiments
  - Supercritical drying
  - Scanning electron microscopy
  - Atomic force microscopy
  - Proton conductivity
- QUANTIFICATION AND STATISTICAL ANALYSIS
- ADDITIONAL RESOURCES

SUPPLEMENTAL INFORMATION

Supplemental information can be found online at https://doi.org/10.1016/j.isci.2021.102947.

ACKNOWLEDGMENTS

We would like to thank Jason Cope (NOAA), Scott Hamilton, and Matthew Jew (Moss Landing Marine Laboratories) for providing access to expired *H. colliei* specimens for AoL gel extraction. This research used Beamline 7.3.3 of the Advanced Light Source, which is a DOE Office of Science User Facility under contract no. DE-AC02-05CH11231 (Hexemer et al., 2010). MR and MJ acknowledge the Office of Naval Research Award N000141612507 (DURIP), the W.M. Keck Center for Nanoscale Optofluidics, the California Institute for Quantitative Biosciences (QB3), and the Army Research Office under award number W911NF-17-1-0460 for equipment and facilities for supporting the proton conductivity experiments and funding from the

Defense Advanced Research Projects Agency (DARPA) and the Department of the Interior under award No. D20AC00003. Funds were also provided by UC Merced (to CTA) and by a UC Merced Senate award to CTA and LSH.

AUTHOR CONTRIBUTIONS

MP primarily contributed to the design of the research with assistance from other authors; MP, LSH, ACW, MJR, and MJ performed experiments; all authors analyzed data; and MP wrote the manuscript with input from all authors.

CONFLICTS OF INTEREST

The authors declare no competing interests.

Received: February 27, 2021
Revised: June 1, 2021
Accepted: August 2, 2021
Published: September 24, 2021

REFERENCES

Buchtova, N., and Budtova, T. (2016). Cellulose aero-, cryo- and xerogels: towards understanding of morphology control. Cellulose *23*, 2585–2595.

Bureekaew, S., Horike, S., Higuchi, M., Mizuno, M., Kawamura, T., Tanaka, D., Yanai, N., and Kitagawa, S. (2009). One-dimensional imidazole aggregate in aluminium porous coordination polymers with high proton conductivity. Nat. Mater. *8*, 831–836. https://doi.org/10.1038/nmat2526.

Deng, Y., Josberger, E., Jin, J., Rousdari, A.F., Helms, B.A., Zhong, C., Anantram, M.P., and Rolandi, M. (2013). H+-type and OH- -type biological protonic semiconductors and complementary devices. Sci. Rep. *3*, 2481. https://doi.org/10.1038/srep02481.

Djabourov, M. (1988). Architecture of gelatin gels. Contemp. Phys. *29*, 273–297.

Doyle, J. (1967). The 'lorenzan sulphates' - a new group of vertebrate mucopolysaccharides. Biochem. J. *103*, 325–330.

Ganesan, K., Budtova, T., Ratke, L., Gurikov, P., Baudron, V., Preibisch, I., Niemeyer, P., Smirnova, I., and Milow, B. (2018). Review on the production of polysaccharide aerogel particles. Materials (Basel), 2144. https://www.mdpi.com/1996-1944/11/11/2144.

Ganesan, K., Dennstedt, A., Barowski, A., and Ratke, L. (2016). Design of aerogels, cryogels and xerogels of cellulose with hierarchical porous structures. Mater. Des. *92*, 345–355.

Guo, Q.H., Jia, M., Liu, Z., Qiu, Y., Chen, H., Shen, D., Zhang, X., Tu, Q., Ryder, M.R., Chen, H., et al. (2020). Single-crystal polycationic polymers obtained by single-crystal-to-single-crystal photopolymerization. J. Am. Chem. Soc. *142*, 6180–6187. https://doi.org/10.1021/jacs.9b13790.

Haas, J., Ravi Kumar, M.N., Borchard, G., Bakowsky, U., and Lehr, C.M. (2005). Preparation and characterization of chitosan and trimethyl-chitosan-modified poly-(epsilon-caprolactone) nanoparticles as DNA carriers. AAPS PharmSciTech. *6*, E22–E30. https://doi.org/10.1208/pt060106.

Harder, A., Walhorn, V., Dierks, T., Fernandez-Busquets, X., and Anselmetti, D. (2010). Single-molecule force spectroscopy of cartilage aggrecan self-adhesion. Biophys. J. *99*, 3498–3504. https://doi.org/10.1016/j.bpj.2010.09.002.

Harm, S., Hatz, A.-K., Moudrakovski, I., Eger, R., Kuhn, A., Hoch, C., and Lotsch, B.V. (2019). Lesson learned from NMR: characterization and ionic conductivity of LGPS-like Li7SiPS8. Chem. Mater. *31*, 1280–1288.

Hexemer, A., Bras, W., Glossinger, J., Schaible, E., Gann, E., Kirian, R., MacDowell, A., Church, M., Rude, B., and Padmore, H. (2010). A SAXS/WAXS/GISAXS beamline with multilayer monochromator. J. Phys. Conf. Ser. *247*, 012007. https://doi.org/10.1088/1742-6596/247/1/012007.

Hirst, L.S., Pynn, R., Bruinsma, R.F., and Safinya, C.R. (2005). Hierarchical self-assembly of actin bundle networks: gels with surface protein skin layers. J. Chem. Phys. *123*, 104902. https://doi.org/10.1063/1.1961229.

How, M.J., and Jones, J.V.S. (1969). Comparative studies of Lorenzini jelly from 2 species of elasmobranch .I. Preparation of glycopeptides. Carbohydr. Res. *11*, 207. https://doi.org/10.1016/S0008-6215(00)80076-2.

How, M.J., Jones, J.V.S., and Stacey, M. (1970). Comparative studies of Lorenzini jelly from two species of elasmobranch. Carbohydr. Res. *12*, 171–181.

Irvine, J.T., Sinclair, D.C., and West, A.R. (1990). Electroceramics: characterization by impedence spectroscopy. Adv. Mater. *2*, 132–138.

Jalili, J., and Tricoli, V. (2014). Proton conductance at elevated temperature: Formulation and investigation of poly(4-styrenesulfonic acid)/4-aminobenzylamine/Phosphoric acid membranes. Front. Energy Res. *2*. https://doi.org/10.3389/fenrg.2014.00028. https://www.frontiersin.org/article/10.3389/fenrg.2014.00028.

Josberger, E.E., Hassanzadeh, P., Deng, Y., Sohn, J., Rego, M.J., Amemiya, C.T., and Rolandi, M. (2016). Proton conductivity in ampullae of Lorenzini jelly. Sci. Adv. *2*, e1600112. https://doi.org/10.1126/sciadv.1600112.

Kalmijn, A.J. (1974). The detection of electric fields from inanimate and animate sources other than electric organs. In Electroreceptors and Other Specialized Receptors in Lower Vertrebrates, A. Fessard, ed. (Springer Berlin Heidelberg), pp. 147–200. https://doi.org/10.1007/978-3-642-65926-3_5.

Kempster, R.M., McCarthy, I.D., and Collin, S.P. (2012). Phylogenetic and ecological factors influencing the number and distribution of electroreceptors in elasmobranchs. J. Fish Biol. *80*, 2055–2088. https://doi.org/10.1111/j.1095-8649.2011.03214.x.

Maier, J. (2005). Nanoionics: ion transport and electrochemical storage in confined systems. Nat. Mater. *4*, 805–815. https://doi.org/10.1038/nmat1513.

Murray, R.W., and Potts, W.T.W. (1961). The composition of the endolymph, perilymph, and other body fluids of elasmobranchs. Comp. Biochem. Physiol. *2*, 65–75.

Newton, K.C., Gill, A.B., and Kajiura, S.M. (2019). Electroreception in marine fishes: chondrichthyans. J. Fish Biol. *95*, 135–154. https://doi.org/10.1111/jfb.14068.

Ng, L., Grodzinsky, A.J., Patwari, P., Sandy, J., Plaas, A., and Ortiz, C. (2003). Individual cartilage aggrecan macromolecules and their constituent glycosaminoglycans visualized via atomic force microscopy. J. Struct. Biol. *143*, 242–257. https://doi.org/10.1016/j.jsb.2003.08.006.

Pethrick, R.A. (2004). Polymer physics. Polymer International, *53* (Michael Rubinstein and Ralph H Colby Oxford University Press), p. 440. ISBN 019852059X. https://doi.org/10.1002/pi.1472. https://onlinelibrary.wiley.com/doi/abs/10.1002/

pi.14721394-1395. https://doi.org/10.1002/pi.1472.

Phillips, M., Tang, W.J., Robinson, M., Ocampo Daza, D., Hassan, K., Leppert, V., Hirst, L.S., and Amemiya, C.T. (2020). Evidence of chitin in the ampullae of Lorenzini of chondrichthyan fishes. Curr. Biol. *30*, R1254–R1255. https://doi.org/10.1016/j.cub.2020.08.014.

Phillips, R. (2018). Membranes by the numbers. In Physics of Biological Membranes, P. Bassereau and P. Sens, eds. (Springer International Publishing), pp. 73–105. https://doi.org/10.1007/978-3-030-00630-3_3.

Quignard, F., Valentin, R., and Di Renzo, F. (2008). Aerogel materials from marine polysaccharides. New J. Chem. *32*, 1300–1310.

Raschi, W. (1986). A morphological analysis of the ampullae of Lorenzini in selected skates (pisces, Rajoidei). J. Morphol. *189*, 225–247.

Sahin, I., Ozbakir, Y., Inonu, Z., Ulker, Z., and Erkey, C. (2017). Kinetics of supercritical drying of gels. Gels *4*. https://doi.org/10.3390/gels4010003.

Selberg, J., Jia, M., and Rolandi, M. (2019). Proton conductivity of glycosaminoglycans. PloS one *14*, e0202713. https://doi.org/10.1371/journal.pone.0202713.

Soboleva, T., Xie, Z., Shi, Z., Tsang, E., Navessin, T., and Holdcroft, S. (2008). Investigation of the through-plane impedance technique for evaluation of anisotropy of proton conducting polymer membranes. J. Electroanalytical Chem. *622*, 145–152. https://doi.org/10.1016/j.jelechem.2008.05.017.

Stribeck, N. (2007). X-Ray Scattering of Soft Matter (Springer-Verlag).

Tang, W.J., Fernandez, J., Sohn, J.J., and Amemiya, C.T. (2015). Chitin is endogenously produced in vertebrates. Curr. Biol. *25*, 897–900. https://doi.org/10.1016/j.cub.2015.01.058.

Tricas, T.C., Michael, S.W., and Sisneros, J.A. (1995). Electrosensory optimization to conspecific phasic signals for mating. Neurosci. Lett. *202*, 129–132.

Zeng, J.B., He, Y.S., Li, S.L., and Wang, Y.Z. (2012). Chitin whiskers: an overview. Biomacromolecules *13*, 1–11. https://doi.org/10.1021/bm201564a.

Zhang, X., Xia, K., Lin, L., Zhang, F., Yu, Y., St Ange, K., Han, X., Edsinger, E., Sohn, J., and Linhardt, R.J. (2018). Structural and functional components of the skate sensory organ ampullae of Lorenzini. ACS Chem. Biol. *13*, 1677–1685. https://doi.org/10.1021/acschembio.8b00335.

STAR★METHODS

KEY RESOURCES TABLE

REAGENT or RESOURCE	SOURCE	IDENTIFIER
Chemicals, peptides, and recombinant proteins		
Chitin-Binding Domain peptide	New England Biolabs	pYZ205 plasmid was a gift from New England Biolabs & Yinhua Zhang (Addgene plasmid # 104586; http://n2t.net/addgene:104586; RRID:Addgene_104586)
SNAP Alexa Fluor-546	New England Biolabs	Cat#S9132S
MS-222 (Tricaine)	Western Chemical, Inc.	Cat#NC0872873
Proteinase K	ThermoFisher	Cat#EO0492
DAPI (4′,6-Diamidine-2′-phenylindole dihydrochloride)	Sigma-Aldrich	Cat#MBD0015
Coomassie Brilliant Blue	Fisher	Cat#501035935
Experimental models: Organisms/Strains		
Ratfish	Wild Caught, male, 41 cm - Univ. Washington	N/A
Ratfish	Wild Caught adults, both sexes - Moss Landing Marine Lab	N/A
Software and algorithms		
Nova 2.0	Metrohm Autolab	Nova 2.0
Igor Pro	Wavemetrics	Igor Pro

RESOURCE AVAILABILITY

Lead contact

Further information and requests for resources and reagents should be directed to and will be fulfilled by the lead contact, Chris T. Amemiya (camemiya@ucmerced.edu).

Materials availability

This study did not generate new unique reagents.

Data and code availability

- Microscopy images and data reported in this paper are deposited on a Box site and will be shared by the lead contact upon request.
- Small-angle x-ray scattering and electrochemical impedance spectroscopy data are deposited on a Box site and will be shared by the lead contact upon request.
- Any additional information required to reanalyze the data reported in this paper is available from the lead contact upon request.
- This paper does not report original code.

EXPERIMENTAL MODEL AND SUBJECT DETAILS

- In this study, ratfish (*Hydrolagus colliei*) were used for the source of histological preparations and for extraction of AoL gel for microscopy, SAXS, and EIS measurements.
- For histological preparations, one live adult ratfish (41 cm, male) was procured and euthanized, and its tissues were fixed in formalin fixative.
- For SAXS and EIS measurements, pooled gel from > 20 expired and frozen ratfish specimens (mixed sexes) were utilized.

METHOD DETAILS

Biological specimens

A spotted ratfish, *Hydrolagus colliei* (41 cm, male), was collected by Thomas Quinn (University of Washington) on a research cruise in Puget Sound and brought to the Benaroya Research Institute, Seattle, for tissue processing. Additional expired and frozen adult spotted ratfish (males and females) were obtained from Jason Cope (NOAA), Scott Hamilton (Moss Landing Marine Labs, MLML), and Matthew Jew (MLML). All animal work was conducted under approved Institutional Animal Care and Use Committee (IACUC) protocols: IACUC16-014 (Benaroya Research Institute) and AUP18-0001 (University of California, Merced). Euthanasia of the one ratfish specimen was carried out using tricaine methylsulfonate (Western Chemical Inc., #NC0872873) at 1000 mg/L. Expired and frozen adult spotted ratfish (*Hydrolagus colliei*) specimens were thawed in a refrigerator overnight, and then AoL gel was removed by applying pressure to the pores with gloved fingers or the blunt side of a scalpel, placed in tubes, and stored at -80°C until use.

CBD staining and fluorescence microscopy

Paraffin sections of formalin-fixed *H. colliei* tissues were prepared using standard processing, embedding, and microtomy protocols and stained following protocols described in the study by Phillips et al., 2020, and epifluorescence images were taken using a Leica DMR upright epifluorescent microscope equipped with a SPOT RT Slider cooled 1.4 megapixel color/monochrome CCD camera and an Insight 4 megapixel color CCD camera (Diagnostic Instruments), or a Keyence BZ-X700 microscope workstation equipped with epifluorescence.

To prepare the samples imaged in Figures 2C and 2D, an aliquot of AoL gel from *H. colliei* was placed in a small centrifuge tube. Chitin-binding domain (CBD) probes (Phillips et al., 2020) were diluted in 1X phosphate buffered saline (PBS) and pipetted gently on top of the gel sample and incubated overnight at 4°C. The next day, the CBD liquid was gently replaced with Milli-Q water to wash the specimen. Gel was pulled from the tube, placed on a slide, and then imaged using a Leica DMP fluorescence microscope with a Qimaging Retiga Exi CCD camera.

Gel digestion with proteinase K (for AFM imaging) and analysis by SDS-PAGE

Equal volumes of AoL gel and water were combined in a tube and vortexed vigorously. Proteinase K was added to a final concentration of 40 μg/μL and incubated for one hour at 50°C. An aliquot was then added to dialysis tubing with MWCO 12-14 KDa (Fisher #21-152-15), dialyzed overnight in 5 L of water at 4°C, and then stored at -20°C until use. For SDS-PAGE, 30 μL of gel sample was combined with 10 μL of reducing buffer and incubated at 95°C for 5 minutes. 1X running buffer was prepared, and 1% SDS was added. Samples were loaded into precast gels (Sigma #PCG2001-10EA) along with marker (Lonza ProSieve Color Protein Marker #BMA50550). Gel was run at 50 V for 20 minutes, then at 100 V for 50 minutes, and then rinsed with DI water. Coomassie Brilliant Blue stain (Fisher #501035935) was poured over gel and incubated for 5 hours. Destain was then added to gel and swirled overnight before pictures were taken.

Gel digestion with proteinase K (for SAXS)

Equal volumes of AoL gel and 1X PBS were combined in a tube and vortexed vigorously. Proteinase K was added to the gel sample to a final concentration of 0.1 μg/μL and incubated at 50°C for one hour. Sample was then dialyzed with 3.5-KDa dialysis tubing in 2 L of water for 5 hours.

Gel digestion with proteinase K (for sonication and AFM)

Equal volumes of AoL gel and buffer (0.1 M Tris + 0.05 M ethylenediaminetetraacetic acid + 0.1% SDS) were combined and proteinase K was added to a final concentration of 40 μg/μL. The solution was incubated at 50°C for an hour and then heated at 60°C for 30 min to denature remaining enzymes. The resulting solution was dialyzed overnight in 5 L of water with 12- to 14-KDa dialysis tubing (Fisher #21-152-15). Lastly, the sample was sonicated on the continuous setting on ice for 20 minutes.

Ultracentrifugation of AoL gel

Several milliliters of AoL gel were dialyzed overnight in 3.5-KDa dialysis tubing in 5 L of water at 4°C to remove salts. A thick-walled polycarbonate lidless centrifuge tube was filled with dialyzed gel (~500 μL) and then spun at ~300,000-400,000 x g for 16 hours at 4°C with a TLA-120.1 Beckman Coulter rotor in an Optima

Max-XP ultracentrifuge. A sample of Proteinase-K-digested gel was put into a centrifuge tube and also spun at ~300,000-400,000 x g for 16 hours.

Synchrotron X-ray experiments

SAXS experiments were carried out at Lawrence Berkeley National Laboratory's (LBNL) Advanced Light Source (ALS) on Beamline 7.3.3. Synchrotron radiation provides a high-intensity, collimated x-ray beam, ideal for studying poorly ordered, dilute isotropic aqueous materials such as biological gels. Previously prepared gel samples were inserted into 1.5-mm quartz x-ray capillaries (Charles Supper Inc.) by gentle centrifugation and mounted in the beam path in a transmission configuration. Capillaries were mounted in a motorized translation stage, allowing precise control of capillary position in a plane perpendicular to the beam direction. A water-filled capillary was included to obtain scattering data for the water background of the gels. A capillary containing silver behenate was included for beam center calibration and determining the sample to detector distance which was 3529.37 mm. To perform the scattering experiments, we used an approximately 300 μm (H) x 700 μm (W) beam at 10 keV and exposed the gels for 2.0 seconds per capillary at several different positions to obtain the most intense scattering pattern for analysis. The scattering patterns were recorded on a Pilatus 2M detector for analysis. The pixel size of the detector was 172 μm^2.

Data analysis was performed using the Nika and Irena macros in Igor Pro by WaveMetrics. The patterns showed diffuse scattering and rings of approximately uniform intensity (no significant alignment was observed) and were radially integrated to obtain 1D intensity plots as a function of q, the scattering vector. To perform the integration, we selected sectors on the scattering pattern image at various azimuthal angles and angular widths. The intensity plots shown were taken from the integration of sectors at an azimuthal angle of 60 degrees with an angular width of 20 to 40 degrees. The full 2π scattering pattern was not accessible on this particular beamline setup, so sector widths were chosen to produce data with a high signal-to-noise ratio, while optimizing the q range for our material. The Igor wave arithmetic tool was used to subtract the water background.

Supercritical drying

An AoL gel sample was placed in 3.5-KDa dialysis tubing, sealed on both ends using dialysis clamps, and left in ethanol 200 proof for several hours (in most cases, overnight). Dialysis tubing became very stiff, and little liquid remained inside after ethanol incubation. Often, white precipitate was observed coating the inside of the tube. Dialysis clamps were replaced with twist ties before introduction to the supercritical drying system. Supercritical drying was performed using a Denton Vacuum, Inc supercritical drying system. The chamber was flushed with liquid CO_2 until no ethanol smell was observed in the effluent followed by a 2-hour soak in pressurized liquid CO_2 to allow exchange of ethanol inside the dialysis tubing. Phase change to supercritical CO_2 was achieved by heating the chamber to ~50°C (reaching pressure of ~1400 psi). Final drying was achieved by reducing sample chamber pressure, allowing the supercritical CO_2 to transition to the gas phase. Samples were stored under vacuum until imaging.

Scanning electron microscopy

AoL gel samples were ambiently dried on a freshly cleaved piece of mica attached to an aluminum stub using a piece of double-sided carbon tape. For supercritical dried samples, a piece of double-sided carbon tape was stuck onto aluminum stubs and then pressed onto the inside of the dialysis tubing containing supercritical dried samples. SEM was performed using the Zeiss Gemini500 FEG-SEM at the Imaging and Microscopy Facility of University of California, Merced. Beam landing energy of 500 eV and secondary electron detection were used.

Atomic force microscopy

AoL samples were dropped directly onto freshly cleaved sheets of mica and dried ambiently in a covered box for several hours. AFM was performed using a Veeco Innova instrument in tapping mode. Probes with a spring constant of 40 N/m (Tap300Al-G, Budget Sensors) were used to image air-dried samples drop-cast on freshly cleaved mica to obtain topographical, amplitude, and phase images in air. Images were collected at a scan rate of 1 line per second at room temperature.

Proton conductivity

Samples of dialyzed gel and proteinase-K-treated dialyzed gel were brought to UC Santa Cruz where analyses were performed. The two-terminal devices used in EIS measurements were fabricated on a glass wafer (Figure 5A). Prior to device fabrication, the substrates were cleaned by sequential sonication in acetone, isopropyl alcohol, and water. Then, a 10-nm titanium adhesion layer overlaid with a 100-nm gold was electron-beam evaporated onto the clean substrates through a shadow mask. The dimensions of the paired electrodes were 1 cm wide by 2 cm long with an interelectrode separation of 50 μm. A polydimethylsiloxane (PDMS) well was made with a 4-mm biopsy punch and bonded to the glass wafer to define the geometry of the gel. The devices were completed by drop casting the native *H. colliei* AoL gel and digested gel directly into the PDMS well, and the resulting films were allowed to dry in air (Figure S5). We hydrated the samples by incubating them in a home-made sealed chamber at 90% relative humidity (RH) at room temperature for 2 hours with D_2O or H_2O. After incubation, Nyquist plots were recorded using Autolab PGSTAT128N between 100 kHz and 0.1 Hz at 10 mV amplitude and analyzed using Nova 2.0 software. Then, we calculated the conductivity (σ) using the following equation: $\sigma = L / R_b A$ where A is the cross-sectional area given by the width of the contact (4 mm) multiplied by the thickness of the sample as measured with atomic force microscopy (2.7 $\pm$ 1.9 μm for ratfish gel, 0.46 $\pm$ 0.27 μm for digested ratfish gel), L is the device length or electrode separation (50 μm), and R_b is the value of resistance obtained from the equivalent circuit we mentioned earlier.

QUANTIFICATION AND STATISTICAL ANALYSIS

None outside of measurements generated by commercial software packages used for analysis of SAXS and EIS data.

ADDITIONAL RESOURCES

None generated.